THE JOURNAL OF PHYSICAL CHEMISTRY B

Article

pubs.acs.org/JPCB

Dynamics of Solvation and Rotational Relaxation of Coumarin 480 in Pure Aqueous-AOT Reverse Micelle and Reverse Micelle Containing Different-Sized Silver Nanoparticles Inside Its Core: A Comparative Study

Palash Setua,[†] Chiranjib Ghatak,[†] Vishal Govind Rao,[†] S. K. Das,[‡] and Nilmoni Sarkar*[,†]

[†]Department of Chemistry, Indian Institute of Technology, Kharagpur 721302, West Bengal, India

[‡]Variable Energy Cyclotron Centre, 1/AF, Bidhan Nagar, Kolkata 700064, West Bengal, India

Supporting Information

ABSTRACT: In this work, we have synthesized different-sized silver nanoparticles in an aqueous-AOT reverse micellar system under the same condition by choosing different reduction processes. We chose two different reducing agents, glucose (mild) and sodium borohydride (strong). In the glucose reduction process, we obtained smaller size nanoparticles in comparison to the nanoparticles obtained in the borohydride reduction process under the same condition. Solvation dynamics study showed that reverse micellar aggregated structures were present after the nanoparticles' formation in a perturbed state. Nanoparticles inside the reverse micellar core were responsible for this perturbation. Larger size nanoparticles were triggering larger perturbation than the smaller size nanoparticles. These changes in perturbation were also reflected clearly in solvation dynamics and rotational relaxation measurements.

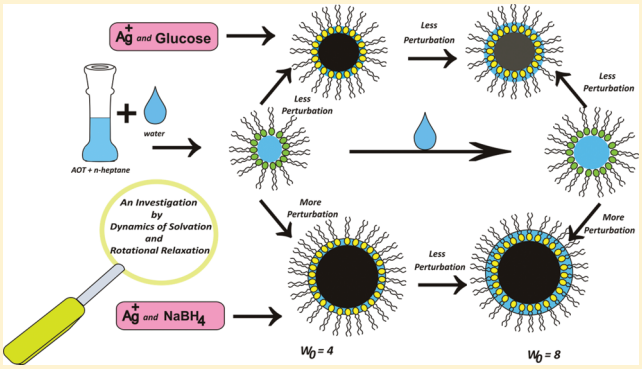

1. INTRODUCTION

Synthesis of nanoparticles can be achieved by different methods using a physical, chemical, or biological approach.[1−3] Among them, reverse micelle or microemulsion-assisted nanoparticle synthesis is one of the most popular techniques. Reverse micellar aggregates act as a soft template during the nanomaterial formation process. As the process involves a template, it will have direct influence on the synthesized nanoparticles. By using a suitable template, one can easily incorporate desired morphology in the synthesized material. Templating effects are also used to control the shape and size of the nanoparticles.[4] The idea behind the formation of reverse micelle is very simple and straightforward. Long-chain amphiphilic molecules (whose one end is polar and the other end is nonpolar), normally called as surfactant molecules, are dissolved in nonpolar solvent within a certain concentration range. The polar end of the amphiphilic molecules try to shade them from the unfavorable nonpolar solvent interaction. For that purpose, they form an aggregated structure where all the polar ends remain directed toward the core of the aggregates. This polar core is used to store the polar solvent as a nano reactor for different purposes and also to synthesize stable nanoparticles.[5−7] Each kind of templating media has its specific type of influence on the nanoparticles morphology. But, as it is a "soft template", some variation in the size and morphology is observed depending on the specific process or reaction which is adopted during the nanoparticle formation. At the initial state, the template affects the nanoparticle's formation, but, at the end, the formed particle also modifies the template structure. This may be called as a feedback effect. Nanoparticles having different size and morphology perturbed the reverse micellar structure to a different extent.[8,9] Numerous studies have been done and a lot of study is still going on the characterization of the different pure reverse micellar structure.[10,11] Some groups are working on the properties of the water when it remains confined inside the reverse micellar core.[12−23] Polar solvents show surprisingly different properties when they are confined inside the reverse micelle. Those properties are strikingly different from the normal bulk properties of that solvent. Those property changes are directly related to the characteristics of the reverse micelles. So these changes also give valuable information about the aggregated structure and its change. The dynamics of solvation and rotational relaxation is an important tool in this field.[33] In this process, a solvatochromic probe molecule is inserted into the reverse micellar phase and then a detailed measurement of its fluorescence properties is carried out. Those results are analyzed to get valuable information about its residing

Received: April 1, 2011
Revised: February 28, 2012
Published: March 1, 2012

environment and the surrounding solvent properties because the fluorescence response of these probe molecules is directly affected by the properties of the surrounding solvent molecules and the probe's environment. To the best of our knowledge, there is no report of any work (except our initial work[28]) that analyzes the state of the perturbed reverse micellar aggregates after the formation of the nanoparticles inside its core or the characteristics of the polar solvent which remained present inside the reverse micelle.

In our previous study on the aqueous-AOT (aerosol-OT, sodium bis(2-ethylhexyl) sulfosuccinate) reverse micelle in a single situation, we showed that reverse micellar aggregate structure was drastically changed by the formation of the silver nanoparticle inside its core.[28] Those changes were reflected in the fluorescence measurement and were monitored by the dynamics of polar solvation and rotational relaxation. We also carried out a detailed study on nonaqueous ethylene glycol reverse micellar system containing silver nanoparticles.[29] To boost the knowledge and to get more information about these complicated systems, we designed this present study. In this article, we report a detailed study on perturbed water/AOT/isooctane reverse micellar system by creating different-sized silver nanoaprticles inside its core in different environments. For this purpose, we performed our study at two different w values (w value is the molar ratio of polar solvent to surfactant), $w = 4$ and $w = 8$. Changes in the w value will create different environments inside the reverse micellar aggregates. To achieve the goal of different nanoparticle size, we used two different reducing agents to reduce the silver ion: one is glucose which belongs to the category of mild reducing agent and the other is sodium borohydride which is a strong reducing agent. Finally, we used coumarin 480 (C-480) probe molecule for the dynamics of solvation and rotational relaxation study which has a better solubility in aqueous environment than the previously used coumarin 153 (C-153) probe molecule. The better solubility ensures better understanding of the reverse mcellar core environment because solvation dynamics is an invasive technique and probe location has a great impact on its result. Another important point which we should mention here is that synthesized silver nanoparticles in all conditions were non-fluorescent in nature. If it were fluorescent in nature then the study would be very complicated.

2. EXPERIMENTAL SECTION

2.1. Materials Used. Coumarin 480 (C-480) (laser grade from Exciton) was used as received (for structure, see Scheme 1). AOT (dioctylsulfosuccinate, sodium salt, Aldrich) was

Scheme 1. Structure of Coumarin 480 Molecule

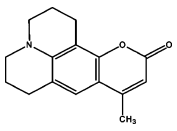

purified by standard procedure[18,19] (for structure, see Scheme 2). n-Heptane of spectroscopic grade (spectrochem) was freshly distilled over calcium hydride (Spectrochem) before use. D-Glucose and sodium borohydride (extrapure) were purchased from Sisco Research Laboratories, Mumbai, India, and were used without further purification. Silver nitrate (analytical reagent) was purchased from Qualigens Fine Chemicals, Mumbai, India, and was used as received. The

Scheme 2. Structure of AOT Molecule

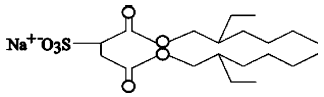

concentration of C-480 maintained in all the measurements was 5×10^{-5} M and that of AOT was 0.09 M. Throughout the work, we used triple distilled water where it was required.

2.2. Reverse Micellar Solution Preparation. Normal reverse micellar solutions were prepared using a stock solution of AOT in n-heptane. Concentration of AOT in the solution was 0.09 M. We made the solution by dissolving an exact amount of AOT in a specific volume n-heptane by direct weighing. Then we added the required amount of triple distilled water to attain the specific w value. To the prepared AOT reverse micellar solution with coumarin 480 probe molecule, we prepared a 2×10^{-3} M stock solution of C-480 in methanol by accurate weighing. Then we took its required volume and poured it in volumetric flask to get the concentration mark of 5×10^{-5} M for a specific volume of AOT−n-heptane mixture and perfectly dried it. Then we added that specific volume of AOT−n-heptane mixture into that volumetric flask and shook it well to homogenize it. Solubilization of water into the reverse micellar solution was done by direct hand shaking. w_0 value of reverse micellar solution is nothing but the molar ratio of polar solvent (reverse micellar core solvent) to surfactant, i.e., in this case $w_0 = [H_2O]/[AOT]$.

2.3. Preparation of Reverse Micellar Solution Containing Silver Nanoparticles. For nanoparticles synthesis, we prepared a stock solution of silver nitrate in water having a silver ion concentration of 1 M, a glucose solution in water having glucose concentration of 1.1 M, and a sodium borohydride solution in water with a molar strength of 1 M. To prepare silver nanoparticles in reverse micellar solution at a specific w_0 value using glucose as mild reducing agent, we prepared two independent same w_0 value reverse micellar solutions, one containing silver ion and the other containing glucose, using the probe containing AOT−n-heptane mixture. We kept the concentration of silver ion and glucose in those two reverse micellar solutions such that after mixing the value became 1×10^{-3} and 1.1×10^{-3} M, respectively. We chose 1 mM silver ion concentration in both the systems after complete standardization because it was the maximum concentration limit that was acceptable by the systems without hampering the produced nanoparticle solution's stability. In all the cases, volume requirement of the silver and glucose stock solution to prepare the reverse micellar solution containing silver ion and glucose was less than the total requirement of water to reach the each w_0 value. The rest of the water requirement was fulfilled by the direct addition of triple-distilled water. Finally, we mixed these two reverse micellar solutions and kept the reverse micellar mixture in a temperature bath for 2 days (∼52 h), keeping the temperature fixed at 56 ± 2 °C.

During this period, we took the necessary precautions and tightly sealed the mouth of the pot such that no liquid could escape by vaporization. In the final state, the colorless solution turned a beautiful yellow color due to the formation of silver nanoparticles. Finally, we removed the solutions from the temperature bath and kept them at normal temperature for about 8 h. Then we used this solution for solvation dynamics study. TEM analysis was also done from this solution.

dx.doi.org/10.1021/jp203043k | J. Phys. Chem. B 2012, 116, 3704−3712

In the case of the sodium borohydride reduction method, all the initial and final process steps were the same except the temperature bath heating stage because sodium borohydride is a strong reducing agent and it can reduce the silver ion at room temperature within a minute, and the concentration ratio of silver ion to reducing agent which was 1:1. In both systems we used 1 mM silver ion concentration because it was the maximum silver ion concentration that could be used without hampering the nanoparticle solutions' stability.

To get a rough idea about the number of reverse micellar aggregates and the number of nanoparticles present in the reverse micellar solution, we refer our readers to our initial work[28] where we already discussed it in detail.

We prepared the silver nanoparticles in reverse micellar solution keeping all the conditions same but without using coumarin 480 probe molecule and checked their fluorescence spectra. In both the processes, at all w_0 values the synthesized silver nanoparticles were nonfluorescent.

A normal fluorescence quenching was present in the presence of silver nanoparticles which arises from the heavy metal type of quenching and by competitive absorption of the incident and emitting light by silver nanoparticle. Solvation dynamics was not affected by this process. Additives always have some effect on the reverse micellar aggregates, so in an indirect way they may have some influence, but the nature of the influence will be the same for each series of systems (glucose reduction and borohydride reduction) independently.

We could not study the system with additives incorporated inside the reverse micellar core because in the borohydride reduction process, reaction starts instantly just after mixing. In the glucose reduction process, they were not reacting instantly but a slow change was present.

2.4. Instruments Used. A Shimadzu UV−vis spectrophotometer (model UV1601) and a Spex Fluorolog-3 (model FL3-11) spectrofluorimeter were used to collect absorption and emission spectra, respectively. We corrected the fluorescence spectra for the spectral sensitivity of the instrument. For the steady-state experiment, all samples were excited at 408 nm. The details of the time-resolved fluorescence setup were described in our previous publication.[18,19] In brief, the samples were excited at 408 nm picosecond diode laser (IBH, nanoled), and the signals were collected at the magic angel (54.7°) using a Hamamatsu MCP PMT detector (3809U). The instrument response of our setup was ∼90 ps (full width at half-maximum). The same setup was also used for the anisotropy measurement. The analysis of both the time-resolved decay and the anisotropy data were carried out using the IBH DAS 6 decay analysis software. The temperature was kept at 25 °C for all measurements except dynamic light scattering (DLS). DLS measurements were performed using a Malvern Nano ZS instrument (model No-ZEN3600) equipped with a thermostated sample chamber. All experiments were carried out using a 4 mW He−Ne laser (λ = 632.8 nm) at a scattering angle of 173°. TEM pictures were taken using a (JEOL) JEM-2100 transmission electron microscope operating at 200 keV. Samples of TEM were prepared by blotting a carbon-coated (50 nm carbon film) Cu grid (300 mesh, Electron Microscopy Science) with a drop of the Ag microemulsion and allowed to dry. We constructed histograms manually by measuring the individual particle diameter with the help of Image-J software. We measured 250−300 particles for the construction of the size distribution histogram for each w_0 value.

3. RESULTS

3.1. DLS Measurement of the Reverse Micellar Solution and TEM Picture Analysis. DLS measurements were performed on the pure water/AOT/*n*-heptane reverse micellar solution to get an overall idea about its formation, stability, and structural features. Some groups have already reported the size of aqueous-AOT reverse micelles. Pileni et al. reported that the radius of the aqueous-AOT reverse micellar pool is generally 1.5 times of the w_0 value.[34−36] They have also showed that different aggregate sizes can be obtained by different techniques at the same reverse micellar environment and described their probable reason. SAXS study showed the radii of the reverse micelles was ∼1.5 nm at w_0 = 4 and 2.4 nm at w_0 = 8 but the SANS experiment was showing values of ∼1.5 and 1.8 nm at the two conditions.[36] Kinugasa et al. reported a somewhat different observation. They observed average aggregate diameter ∼2 and 3.5 nm at w_0 = 4 and 8.[37] Baruah et al. reported a radius of 4 nm at w_0 = 12.[10] A larger diameter was reported by Vasquez et al.[38] (5.5 and 9.0 nm at w_0 = 5 and 10). Piletic et al. in their recent DLS study showed that AOT reverse micellar diameters were 1.7, 2.6, and 4.0 nm at w_0 = 2, 5, and 10, respectively.[39] For this reason, we have also measured the DLS size distribution of the reverse micellar aggregates in our own experimental conditions in different environments. Another important thing that is noteworthy to mention here is that we plotted the size distribution histogram in number percentage which is more practical than the intensity distribution plot. These two plots show some difference in their distribution profiles and hence in average diameter value. Most of the previous studies used the intensity distribution profiles. Our DLS results in intensity distribution profile show good agreement with the previously reported value but the number distribution profiles (created from the same scattering intensity result) show values that are smaller than the previously reported values by the other group. DLS values reported here are obtained from the number distribution profile if nothing particular is mentioned with it. To give a clear picture of the deviation, we have given the two DLS distribution profiles (number and intensity) recorded at w_0 = 4 in pure water-AOT reverse micelle in (Supporting Information, Figure 6). Figure 1

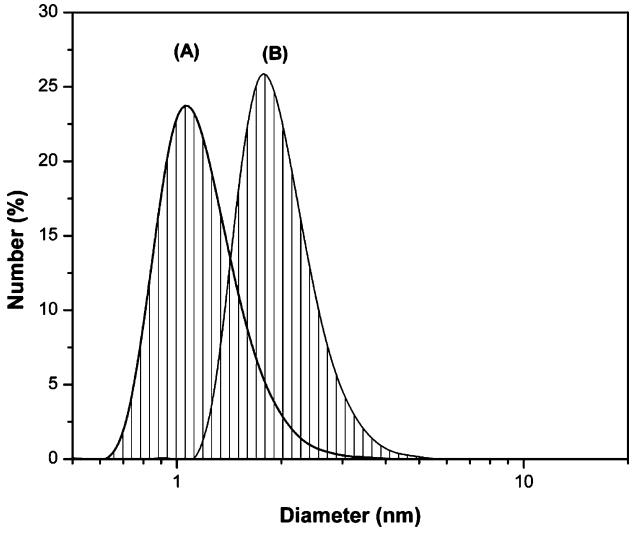

Figure 1. DLS size distribution histogram of pure water/AOT/*n*-heptane (A) at w_0 = 4 and (B) at w_0 = 8.

dx.doi.org/10.1021/jp203043k | J. Phys. Chem. B 2012, 116, 3704−3712

shows the DLS size distribution histogram from the pure water reverse micellar solution. Average diameters of the reverse micellar aggregates were ~1 nm (~2.6 nm in intensity distribution profile) at w_0 = 4 (curve A). The value increased and became ~2 nm (~3.9 nm in intensity distribution profile) at w_0 = 8. We also carried out the DLS measurement on the precursor-loaded reverse micellar aggregates. In the glucose reduction process, the average diameter of the size distribution histogram was increasing. At w_0 = 4, the average diameters of the precursor-loaded reverse micelles were ~3.5 nm and it increased to ~5 nm when we increased the water loading up to w_0 = 8 (see Supporting Information, Figure 1). The w_0 = 4 data of glucose reduction process are taken from our initial study.[28] We could not measure the average diameter of the reverse micellar aggregates after silver ion and sodium borohydride loading because in that process nanoparticles were forming instantly. To get a complete idea of shape, size, and morphology of the synthesized nanoparticles, we carried out the TEM micrograph analysis by directly measuring the particle diameter and constructed the particle size distribution histogram. During this analysis, we avoided the few large agglomerates which are naturally observed in the reverse micellar nanoparticle synthesis process. In the glucose reduction process, the average particle diameter obtained from the TEM picture analysis at w_0 = 4 was ~3.6 nm.[28] We got almost the same average particle diameter (~3.3 nm) at w_0 = 8 (Figure 2). In the sodium borohydride reduction process,

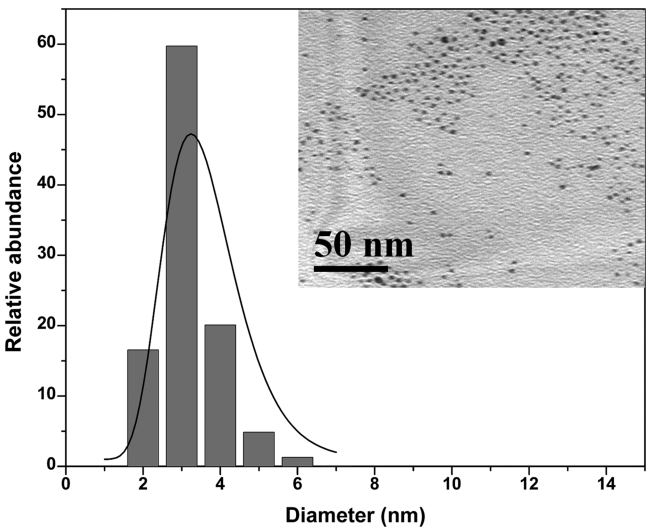

Figure 2. Particle size distribution histogram obtained from TEM picture analysis via glucose reduction process at w_0 = 8.

the average particle diameter obtained from the TEM micrograph analysis was ~7 nm at w_0 = 4 (Figure 3). Also in this process, the average particle diameter remained almost unchanged with the increase in w_0 value from w_0 = 4 to w_0 = 8 (see Supporting Information, Figure 2). The histogram obtained at w_0 = 4 was slightly more polydisperse.

One important point that is noteworthy to mention here is that fast reduction creates a large number of nuclei in a small time, so if we stop the agglomeration process instantly by some surface-capping agent then we will get small-size particles. But in the reverse micelle synthesis process, no surface-capping agent is used. Particles grow naturally inside the reverse micellar core under the protection of the surfactant layer. Surfactant

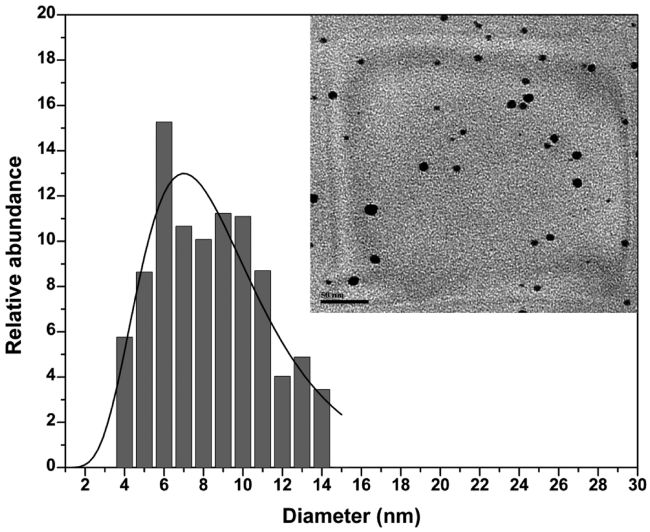

Figure 3. Particle size distribution histogram obtained from TEM picture analysis via sodium borohydride reduction process at w_0 = 4.

molecules are not acting as a surface-capping agent like dodecanethiol. So, one should not apply the concept "fast reduction produces small particle" in this process.

3.2. Steady-State Absorption and Emission Results.

Absorption and emission spectra of C-480 probe molecules were measured in water and *n*-heptane and in different reverse micellar solutions in different conditions. The results are summarized in Table 1. The peak position of C-480 molecules

Table 1. Steady-State Absorption and Emission Spectra of C-480 in Pure *n*-Heptane, Water, and Water/AOT/*n*-Heptane Reverse Micellar System at Different w_0 Values and in Different Environments[a]

system	w_0 value	λ_{abs}(max)/ nm	λ_{emi}(max)/ nm
n-heptane		$(361)^m$, 378	421
water		395	490
water/AOT/*n*-heptane reverse micelle	4	$(361)^m$, 378	473
	8	361^m, 379	480
water/AOT/*n*-heptane with silver nanoparticle via glucose reduction process	4	361, 378	473
	8	361, $(379)^m$	480
water/AOT/*n*-heptane with silver nanoparticle via sodium borohydride reduction process	4	361, $(378)^m$	477
	8	$(380)^m$, 404	488

[a]Excitation wavelength = 408 nm, maximum intensity peak = $(\ )^m$

in the absorption profile was split into two peaks. So, we reported the two peak positions in the table and mark the maximum intensity peak with "m" in the superscript. In *n*-heptane solvent, the respective peak positions were centered at $(361)^m$, 378, and 421 nm. In all other systems, two peak positions of the absorption profile (though their individual intensity was changing) remained unchanged except at w_0 = 8 in silver nanoparticles containing reverse micellar solution in sodium borohydride reduction process where the respective peak positions were $(380)^m$ and 404 nm. The emission maximum of C-480 in pure water/AOT/*n*-heptane reverse

dx.doi.org/10.1021/jp203043k | J. Phys. Chem. B 2012, 116, 3704–3712

Table 2. Rotational Relaxation Parameters of C-480 in Normal Water Reverse Micelle and in Water Reverse Micelle Containing Silver Nanoparticles Prepared Using Different Reduction Methods

system	w_0	r_0	a_{1r}	a_{2r}	τ_{1r} (ns)	τ_{2r} (ns)	$\langle\tau_r\rangle^a$ (ns)^a ($\pm$0.01)
n-heptane		0.21	1.00		0.09		0.09
water/AOT/*n*-heptane reverse micelle	4	0.36	0.49	0.51	0.37	1.97	1.18
	8	0.38	0.58	0.42	0.29	1.65	0.86
water/AOT/*n*-heptane reverse micelles with silver nanoparticles using glucose as reducing agent	4	0.33	0.36	0.64	0.46	2.04	1.47
	8	0.36	0.55	0.45	0.32	1.78	0.97
water/AOT/*n*-heptane reverse micelle with silver nanoparticles using sodium borohydride as reducing agent	4	0.31	0.40	0.60	0.41	2.27	1.52
	8	0.32	0.59	0.41	0.45	2.18	1.16

$^a\langle\tau_r\rangle^a = a_{1r}\tau_{1r} + a_{2r}\tau_{2r}$.

Table 3. Decay Parameter of $c(t)$ for C-480 in Normal Water Reverse Micelle and in Water Reverse Micelle Containing Silver Nanoparticles Prepared Using Different Reduction Methods

system	w_0	$\Delta\nu^a$ (cm^{-1})^a	a_1	a_2	τ_1 (ns)	τ_2 (ns)	$\langle\tau\rangle$ (ns)	missing component (%)
water/AOT/*n*-heptane reverse micelle	4	1455	0.75	0.25	0.43	10.89	3.04	~52
	8	930	0.85	0.15	0.38	16.12	2.74	~70
water/AOT/*n*-heptane reverse micelle with silver nanoparticles using glucose as reducing agent	4	1090	0.62	0.38	0.90	10.32	4.48	–
	8	985	0.82	0.18	0.48	16.39	3.34	–
water/AOT/*n*-heptane reverse micelle with silver nanoparticles using sodium borohydride as reducing agent	4	1177	0.67	0.33	0.75	13.90	5.08	–
	8	790	0.77	0.23	0.41	18.74	4.62	–

$^a\Delta\nu^a = \nu_0 - \nu_\infty$, $\langle\tau\rangle = a_1\tau_1 + a_2\tau_2$.

micelles was 473 nm at w_0 = 4 and shifted to 480 nm at w_0 = 8. The emission maximum of C-480 in water/AOT/*n*-heptane reverse micellar solution containing silver nanoparticles prepared via glucose reduction process was also centered at 473 nm at w_0 = 4 and shifted to 480 nm at w_0 = 8. In the reverse micellar solution containing silver nanoparticles via borohydride reduction process, emission peak positions were at 477 and 488 nm at w_0 = 4 and w_0 = 8, respectively. For more information about the silver nanoparticle absorption spectra, the reader can consult the previous studies of Pileni et al.[36]

3.3. Time-Resolved Anisotropy Results. Time-resolved anisotropy result gives valuable information about the probe location in a system.

We also carried out the time-resolved fluorescence anisotropy measurements of C-480 probe in the water/AOT/*n*-heptane reverse micellar system in different conditions. Time-resolved fluorescence anisotropy was calculated using the following equation

$$r(t) = \frac{I_{\parallel}(t) - GI_{\perp}(t)}{I_{\parallel}(t) + 2GI_{\perp}(t)} \quad (1)$$

where G represents the correction factor of the detector sensitivity to the polarization direction of the emission. In our instrument, the value of G is 0.6. $I_{\parallel}(t)$ and $I_{\perp}(t)$ are the fluorescence decays polarized parallel and perpendicular to the polarization of the excitation light, respectively. The results obtained are summarized in Table 2. We were getting an anisotropy decay time of ~90 ps in pure *n*-heptane solvent. In pure water/AOT/*n*-heptane reverse micelles at w_0 = 4 the value was 1.18 ns. With increasing water content at w_0 = 8, the value became 0.86 ns. In the water/AOT/*n*-heptane reverse micelle containing silver nanoparticles (prepared via glucose reduction), the values were 1.47 and 0.97 ns at w_0 = 4 and w_0 = 8, respectively. When we created a similar system using borohydride as reducing agent, the values became 1.52 and 1.16 ns at w_0 = 4 and w_0 = 8, respectively.

3.4. Dynamics of Solvent Relaxation. Solvation dynamics study was carried out in the water/AOT/*n*-heptane reverse micellar system at different w values in different environments by measuring the time-resolved decay of C-480 molecules at different wavelengths. The time-resolved emission spectra were constructed by the procedure proposed by Fleming and Maroncelli.[26] The solvent relaxation dynamics was monitored by the solvent response function defined as

$$c(t) = \frac{\nu(t) - \nu(\infty)}{\nu(0) - \nu(\infty)} \quad (2)$$

where $\nu(t)$, $\nu(0)$, and $\nu(\infty)$ are the peak frequencies at time t, time zero, and time infinity. The peak frequencies were calculated from the TRES. During this TRES construction we observed an uncertainty around $\pm$100 ps. This uncertainty was also included in the points during the $c(t)$ curve construction. To get a clear idea about the TRES, we have given a representative TRES spectrum in Figure S3 in the Supporting Information. Solvent relaxation times observed from the solvent correlation function $c(t)$ are summarized in Table 3. We were getting an average solvation time of 3.04 ns in the case of pure water/AOT/*n*-heptane reverse micellar system at w_0 = 4. Average solvation time was decreasing with increasing water content and became 2.74 ns at w_0 = 8. In the case of silver nanoparticles containing the reverse micellar system (prepared via glucose reduction), the values were 4.48 and 3.34 ns at w_0 = 4 and w_0 = 8, respectively. Normally, we get single-exponential decay at low w_0 value and then it becomes biexponential in the high w_0 range. But here we were getting biexponential even at w_0 = 4. Weightage contribution of the long component in the overall solvation time was decreasing but the numerical value was higher at w = 8. This was a direct consequence of the very

dx.doi.org/10.1021/jp203043k | J. Phys. Chem. B 2012, 116, 3704–3712

long and flat taillike part of the $c(t)$ decay profile at $w = 8$ (Figure 7). In the case of sodium borohydride reduced silver nanoparticles reverse micellar system the values became 5.08 and 4.62 ns at $w_0 = 4$ and $w_0 = 8$, respectively. Our instrument response function is broad (~90 ps). So we could not monitor the total solvation dynamics. For that reason we calculated the $\nu(0)$ frequency according to the concept proposed by Fee and Maroncelli.[38] Using that value, we calculated the percentage of the missing component observed in pure water/AOT/*n*-heptane system. The percentage of the missing component was ~52% at $w_0 = 4$. The value was increasing with water loading and became ~70% at $w_0 = 8$. It will help the reader to get a picture about the percentage of the solvation dynamics process we are missing and which portion is being taken care of in this work.

4. DISCUSSION

All the DLS size distribution histograms obtained in the DLS measurement were symmetrical, low polydispersity with one peak maximum. This symmetrical distribution and absence of more than one peak or shoulder-like portion indicates the presence of spherical, independent, and stable reverse micellar aggregates. The aqueous reverse micellar system created here was also following the normal AOT−water reverse micellar nature. At $w_0 = 4$ the average reverse micellar diameter was ~1 nm. This value was increasing with water loading and became ~2 nm at $w_0 = 8$ (Figure 1). Incorporation of foreign material perturbs the reverse micellar state. For that reason we measured the DLS size distribution histogram of the reverse micellar aggregates containing silver ion and glucose. Reverse micellar size was increasing in both w_0 values. At $w_0 = 4$ the average diameter became ~3.5 nm[28] and at $w_0 = 8$ it became ~5.5 nm (Supporting Information, Figure S1). DLS measurement of the precursor-loaded reverse micelle in the sodium borohydride reduction process was not possible because sodium borohydride was instantly reducing the silver ion, though Abel et al.[40] reported comparatively larger reverse water−AOT reverse micellar size in their study. We are mentioning it as a different view from ours.

TEM micrograph obtained from the TEM analysis was clearly showing the independent spherical particle of silver. In the glucose reduction process, the average particle diameter at $w_0 = 4$ was ~3.7 nm.[28] With increasing w_0 value (up to $w_0 = 8$), the average diameter of the synthesized particles was not changing. We obtained an average diameter ~3.3 nm at $w_0 = 8$ (Figure 2). Both the results may be considered as identical within experimental variation. In the borohydride reduction process, the average particle diameter obtained was ~7 nm at $w_0 = 4$ (Figure 2). The higher particle diameter obtained in this process was the direct consequence of the use of the stronger reducing agent sodium borohydride which triggers a very fast reaction process. At higher w_0 value, i.e., at $w_0 = 8$, the average particle diameter remained unchanged (Supporting Information, Figure S2). The only visible difference observed between the two histograms was polydispersity. At $w_0 = 4$, synthesized particles were more polydisperse than at $w_0 = 8$. Similar higher polydispersity at lower w_0 value was also observed in previous work.[30] This might be due to the very small reverse micellar core size to accommodate the nanoparticles. So, from these observations it is clear that AOT−reverse micellar aggregates were acting as a template to prepare and stabilize the silver nanoparticles. They were also controlling their size in a different way when we used a different reduction method but were not influencing the size in a specific process with the change in w_0 value within the w_0 range from 4 to 8.

We observed absorption and emission peaks of C-480 molecules in *n*-heptane at $(361)^m$, 378, and 421 nm. In the case of pure water−AOT reverse micellar solution at $w_0 = 4$, absorption peak positions remained unchanged but fluorescence peak maximum was shifted to 473 nm. This was clearly showing the solvent-sensitive behavior of the C-480 probe molecule as well as the formation of the AOT−water reverse micellar aggregates (see Table 2). At $w_0 = 8$ we observed a clear rise at the red end of the absorption peak and also a red shift in the fluorescence maxima (480 nm), which indicated that more and more probe molecules were entering into the reverse micellar aggregates with increase in water loading. It was also indicating that reverse micellar environment was also changing with water loading. In the glucose reduction process, the individual peak position in the absorption remained unchanged though their intensity was changing with w_0 value. Absorption profiles (at $w_0 = 4$ and $w_0 = 8$) changed shape because the silver nanoparticle's absorption spectrum was merged with them. Fluorescence spectra were almost unchanged both in shape and in position from their previous pure reverse micellar counterparts. Change in shape and position in absorption and emission spectra was more prominent in the borohydride reduction process (Figure 4). At $w_0 = 4$ absorption and emission peaks were observed at 361, $(378)^m$, and 477 nm. At $w_0 = 8$, the changes were more prominent. The absorption and emission peaks were shifted to $(380)^m$, 404, and 488 nm. There was always some contribution in the deformation (in shape) of the C-480 absorption peak from the nanoparticles' absorption but fluorescence spectra were free from this interference because nanoparticles were nonfluorescent. These results were clearly showing that normal reverse micellar structure were perturbed in the presence of silver nanoparticles inside the reverse micellar core and this perturbation was more in the sodium

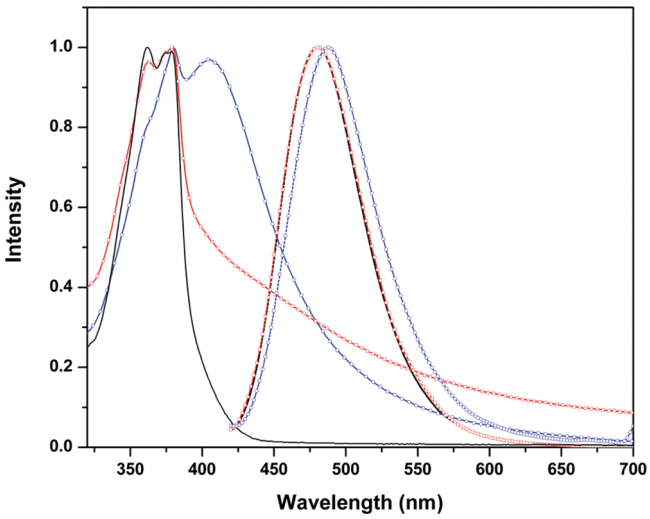

Figure 4. Absorption and emission spectra of C-480 in water/AOT/*n*-heptane pure reverse micelle and reverse micelle containing silver nanoparticles at $w_0 = 8$. Significance of the symbols used: absorption spectra in pure water reverse micelle (—), absorption with silver nanoparticles prepared via glucose reduction (−□−), and absorption with silver nanoparticles prepared via the sodium borohydride reduction method (−○−). Dashed lines with the same symbols represent the respective emission spectra.

dx.doi.org/10.1021/jp203043k | J. Phys. Chem. B 2012, 116, 3704−3712

borohydride reduction method due to the formation of larger nanoparticles.

Steady-state analysis of absorption and emission spectra already revealed that the reverse micellar structures were forming and were present after the nanoparticles' formation, though in a changed state. Further confirmation was obtained from the more accurate time-resolved fluorescence anisotropy analysis. In pure *n*-heptane, we got an anisotropy value (average anisotropy relaxation time) of ~90 ps and the decay was single exponential. In pure water−AOT reverse micellar system with w_0 = 4, the anisotropy decay was biexponential with the time constants of 0.37 and 1.97 ns and the average anisotropy relaxation time is 1.18 ns. So an increase in the anisotropy value was clearly indicating that the probe molecules were partitioned into the reverse micellar aggregates and they were sensing a more restricted environment. Biexponential nature can be explained by considering two types of probe location: one is the interfacial region of the aggregates (responsible for slower component) and the other is reverse micellar core (source of faster component). At w_0 = 8, the anisotropy value decreased and became ~0.86 ns. This decrease showed that, with increasing w_0 value (increase in reverse micellar size), probe molecules were experiencing a less restricted environment which was reflected in the decreased contribution of the slow and increased contribution of the fast component (Figure 5). In

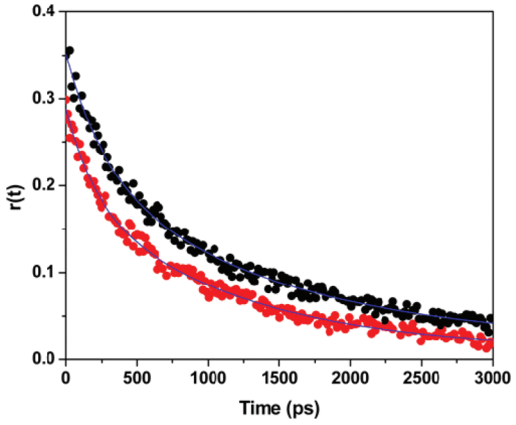

Figure 5. Decay profile of anisotropy in pure water/AOT/*n*-heptane reverse micellar system. Black circles represent w_0 = 4 and red circles w_0 = 8. Blue line indicates the fit.

silver nanoparticles containing reverse micellar system prepared via the glucose reduction method, we got an anisotropy value of 1.47 ns. The value was increased due to an increase in the numerical value of the slow component and its contribution. This was directly concerned with the constraint imposed by the silver nanoparticles present inside the reverse micellar core. With increasing w_0 value (at w_0 = 8), the constraint was relieved and we got a lower anisotropy value of ~0.97 ns. In the case of borohydride reduction process at w_0 = 4, this constraint was maximum due to the presence of larger nanoparticles (average diameter ~7 nm) and the smallest reverse micellar size (~1 nm). We got the largest anisotropy value of ~1.52 ns in this condition. Also in this reverse micellar system, we got a lower anisotropy value, ~1.16 ns at w_0 = 8, which showed a relief in constraint with increasing reverse micellar size. To get a clear idea about the anisotropy variation, we are giving a picture (Figure 6) where we plotted anisotropy profile of different reverse micellar system (with or without nanoparticles) at w_0 = 4.

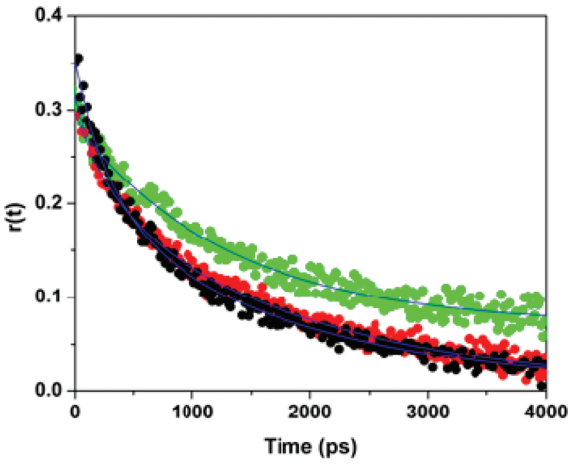

Figure 6. Anisotropy decay profile of C-480 in different AOT−water reverse micellar system (with or without silver nanoparticles) at w_0 = 4. Black circles represent pure water reverse micelle, red circles silver nanoparticles containing reverse micelles prepared via glucose reduction method, and green circles the same via sodium borohydride reduction method. Blue lines indicate the fit.

Results obtained from the solvation dynamics study solely depend on the nature of the polar solvent used. Generally, we obtained very fast solvent response in pure solvent. In water, the response is in the order of femtoseconds time scale,[12,31,32] but their solvent responses are ~1000 times retarded when we incorporate them inside the reverse micellar core. This is due to the nanocage confinement of the solvent by reverse micelle.[13−15,18,19,33] This slow solvation dynamics can be explained by the dynamic exchange model.[20] This model is based on the consideration of the two types of water molecules (free and bound) present in the reverse micellar aggregates. Bound water molecules remain attached with the surfactant headgroup through hydrogen bonding and are present at the reverse micellar interface region. The rest of the water molecules that remain present inside the reverse micellar core are treated as free water molecules. Bound water is responsible for the slow component of the solvent response due to its restricted movement. Free water molecules are responsible for the comparatively faster component as their motion is less restricted. Any change in their relative population affects the overall solvent response in the same manner, i.e., increase in bound water population increases solvation time, and increase in free water population decreases solvation time. In this study, we have successfully applied this model both in pure and in silver nanoparticles containing revere micellar system. In the case of the pure water−AOT reverse micellar system, we were getting an average solvation time ~3.04 ns at w_0 = 4 (see Table 3) and the value was decreasing and became ~2.74 ns at w_0 = 8. With increasing water loading, the relative population of the free water molecules inside the reverse micellar core increases. As the free water molecules are responsible for the faster component, the relative percentage of the faster component increases and we got faster average solvation time at higher w_0 value. We observed 10% increases (75−85%) in the relative contribution of the faster component when we increased the w_0 value from 4 to 8 (see Table 3). In the case of the perturbed reverse micellar system containing silver nanoparticles (pre-

dx.doi.org/10.1021/jp203043k | J. Phys. Chem. B 2012, 116, 3704−3712

pared via glucose reduction process), we got an average solvation time ~4.48 ns. This value is higher than the previously reported value of average solvation time in pure water reverse micelle at w_0 = 4. Close inspection of the data reveals that this was due to the increase in the relative contribution of the slow component from 25% to 38%. The presence of silver nanoparticles inside the reverse micellar core forces the core water of the reverse micelle to the interface which increases the relative population of the interfacial water. This physically feasible phenomenon successfully explains the increment of the slow component from 25% to 38%. In the borohydride reduction process at w_0 = 4 this perturbation process was more drastic because average size of the synthesized nanoparticles was larger. As a direct consequence of this phenomenon, we got maximum average solvation time ~5.08 ns. In this condition, perturbation was so strong that not only the average solvation but also the absolute value of the slow component was changing (from 10.89 to 13.90 ns). At w_0 = 8 this change in absolute value was smaller (from 16.12 to 18.74 ns), because at this condition pure reverse micellar size was doubled but the average particle diameter was unchanged. In both the process (glucose and borohydride reduction), average solvation time in silver nanoparticles containing reverse micellar system was decreasing with the increase in w_0 value. The decrease was 4.48 to 3.34 ns and 5.08 to 4.62 ns in the case of glucose reduction and borohydride reduction, respectively. This observation can also be explained by the above concept that in both the processes average particle diameter was unchanged with increase in w_0 value but the reverse micellar size was doubled which created comparatively weak perturbation with increasing w_0 value. Another factor which may play a role at high w_0 value is the limitation of the surfactant headgroup to convert the number of water molecule to "bound nature", i.e., the number of the water molecules which remain simultaneously hydrogen bonded with a single surfactant headgroup. So all the water molecules remaining in the interface in the perturbed reverse micellar aggregates at higher w_0 value may act as restricted water molecules considering their previously free nature but will not be converted into bound water. For better understanding to the reader and visual comparison we have constructed the Figures 7 and 8. In Figure 7 we have plotted the solvent response function $c(t)$ of pure water reverse micellar system at w_0 = 4 and w_0 = 8 and in Figure 8 the same solvent response function at w_0 = 8 in three different reverse micellar systems. Another important point that we want to mention here is that one should not compare results of the solvation dynamics study between the two parallel procedures (glucose reduction and borohydride reduction) because in one process we are using a covalent (glucose) and in the other process we are using an ionic (sodium borohydride) reducing agent.

5. CONCLUSION

This work certainly concludes the following facts. It confirms the existence of the most widely used water−AOT reverse micellar aggregates after its use in nanomaterial synthesis as a template and nanoreactor. Reverse micellar structure gets perturbed by the incorporation of the precursor material before the nanoparticles' formation. Different-sized silver nanoparticles can be obtained in the same reverse micellar templating media by changing the nature of the reducing agent used to reduce the silver ion. Another important contribution of this study in the aqueous-AOT reverse micellar field is that in this process (the

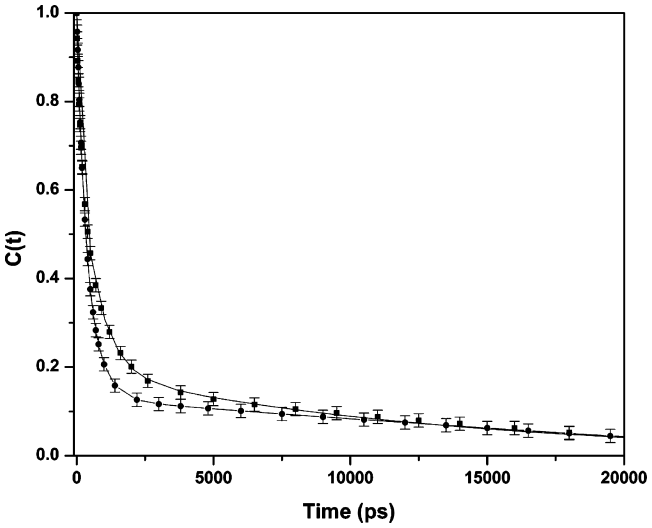

Figure 7. Decay of solvent correlation function $C(t)$ of C-480 molecule in pure water/AOT/*n*-heptane reverse micellar system at w_0 = 4 (black squares) and at w_0 = 8 (black circles).

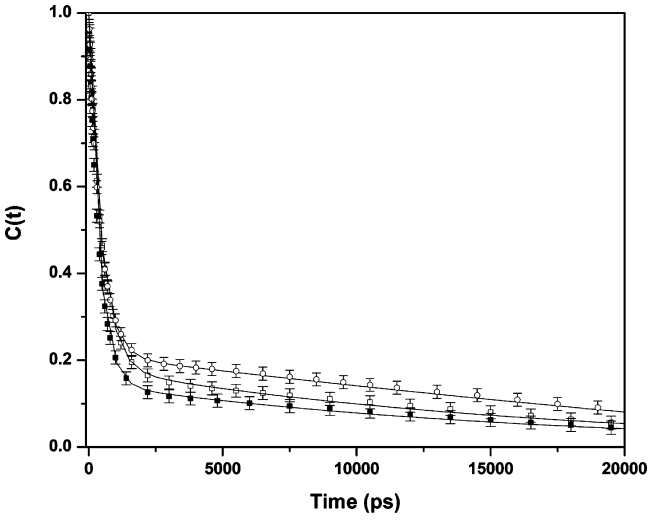

Figure 8. Decay of the solvent correlation function $C(t)$ of C-480 molecule in pure water/AOT/*n*-heptane reverse micellar system and reverse micellar system containing silver nanoparticles prepared via different methods at w_0 = 8. Black squares, pure reverse micelle; open squares, reverse micelle with silver nanoparticles prepared via glucose reduction; and open circles the same prepared via sodium borohydride reduction.

method that we adopted during the nanoparticles synthesis) the synthesized nanomaterial's average size remains almost unchanged and independent of w_0 value up to w_0 = 8. Nanoparticles inside the reverse micellar core perturbed the aggregated structure of the reverse micelle and its core solvent distribution pattern. Dynamic exchange model of solvation dynamics can be successfully applied to these perturbed reverse micellar aggregates. Solvation dynamics and rotational relaxation study showed that smaller size nanoparticles produce lower and larger particles produce higher perturbation. The extent of this perturbation also depends on the mutual difference of the pure reverse micellar size and the size of the residing nanoparticle inside its core.

dx.doi.org/10.1021/jp203043k | J. Phys. Chem. B 2012, 116, 3704−3712

■ ASSOCIATED CONTENT

Supporting Information

Helpful data plots and spectra. This material is available free of charge via the Internet at http://pubs.acs.org.

■ AUTHOR INFORMATION

Corresponding Author

*E-mail: nilmoni@chem.iitkgp.ernet.in. Fax: 91-3222-255303.

Notes

The authors declare no competing financial interest.

■ ACKNOWLEDGMENTS

N.S. is thankful to Council of Scientific and Industrial Research (CSIR), Board of Research in Nuclear Science (BRNS), Government of India, for generous research grants. C.G. and V.G.R. are thankful to CSIR for fellowships.

■ REFERENCES

(1) Sau, T. K.; Rogach, A. L. *Adv. Mater.* **2010**, *22*, 1781−1804.
(2) Narayanan, K. B.; Sakthivel, N. *Adv. Colloid Interface Sci.* **2010**, *156*, 1−13.
(3) Vinodgopal, K.; Neppolian, B.; Lightcap, I. V.; Grieser, F.; Ashokkumar, M.; Kamat, P. V. *J. Phys. Chem. Lett.* **2010**, *1*, 1987−1993.
(4) Uskokovic, V.; Drofenik, M. *Surf. Rev. Lett.* **2005**, *12*, 239−277.
(5) Lopez-Quintela, M. A.; Tojo, C.; Blanco, M. C.; Garcia, R. L.; Leis, J. R. *Curr. Opin. Colloid Interface Sci.* **2004**, *9*, 264−278.
(6) Klyachko, N. L.; Levashov, A. V. *Curr. Opin. Colloid Interface Sci.* **2003**, *8*, 179−186.
(7) Lin, Y. C.; Lee, W. J.; Chao, H. R.; Wang, S. L.; Tsou, T. C.; Guo-Ping, C. C.; Tsai, P. J. *Environ. Sci. Technol.* **2008**, *42*, 3849−3855.
(8) Eastoe, J.; Hollamby, M. J.; Hudson, L. *Adv. Colloid Interface Sci.* **2006**, *128*, 5−15.
(9) Uskokovic, V.; Drofenik, M. *Adv. Colloid Interface Sci.* **2007**, *133*, 23−34.
(10) Baruah, B.; Roden, J. M.; Sedgwick, M.; Correa, N. M.; Crans, D. C.; Levinger, N. E. *J. Am. Chem. Soc.* **2006**, *128*, 12758−12765.
(11) Correa, N. M.; Levinger, N. E. *J. Phys. Chem. B* **2006**, *110*, 13050−13061.
(12) Jimenez, R.; Fleming, G. R.; Kumar, P. V.; Maroncelli, M. *Nature* **1994**, *369*, 471−473.
(13) Nandi, N.; Bhattacharyya, K.; Bagchi, B. *Chem. Rev.* **2000**, *100*, 2013−2045.
(14) Bhattacharyya, K. *Acc. Chem. Res.* **2003**, *36*, 95−101.
(15) Nandi, N.; Bagchi, B. *J. Phys. Chem. B* **1997**, *101*, 10954−10961.
(16) Shirota, H.; Segawa, H. *Langmuir* **2004**, *20*, 329−335.
(17) Shirota, H.; Castner, E. W. Jr. *J. Am. Chem. Soc.* **2001**, *123*, 12877−12885.
(18) Saini, S.; Srinivas, G.; Bagchi, B. *J. Phys. Chem. B* **2009**, *113*, 1817−1832.
(19) Bhowmick, S.; Saini, S.; Shenoy, V. B.; Bagchi, B. *J. Chem. Phys.* **2006**, *125*, 181102−181107.
(20) Moilanen, D. E.; Levinger, N. E.; Spry, D. B.; Fayer, M. D. *J. Am. Chem. Soc.* **2007**, *129*, 14311−14318.
(21) Samanta, A. *J. Phys. Chem. Lett.* **2010**, *1*, 1557−1562.
(22) Mitra, R. K.; Verma, P. K.; Pal, S. K. *J. Phys. Chem. B* **2009**, *113*, 4744−4750.
(23) Hazra, P.; Chakrabarty, D.; Sarkar, N. *Chem. Phys. Lett.* **2003**, *371*, 553−562.
(24) Castner, E. W. Jr.; Maroncelli, M.; Fleming, G. R. *J. Chem. Phys.* **1987**, *86*, 1090−1097.
(25) Maroncelli, M.; MacInnis, J.; Fleming, G. R. *Science* **1989**, *243*, 1674−1681.
(26) Maroncelli, M.; Fleming, G. R. *J. Chem. Phys.* **1987**, *86*, 6221−6239.
(27) Fee, R. S.; Maroncelli, M. *Chem. Phys.* **1994**, *183*, 235−247.
(28) Setua, P.; Pramanik, R.; Sarkar, S.; Seth, D.; Sarkar, N. *J. Phys. Chem. B* **2009**, *113*, 5677−5680.
(29) Setua, P.; Pramanik, R.; Sarkar, S.; Ghatak, C.; Das, S. K.; Sarkar, N. *J. Phys. Chem. B* **2010**, *114*, 7557−7564.
(30) Setua, P.; Chakraborty, A.; Seth, D.; Bhatta, U.; Satyam, P. V.; Sarkar, N. *J. Phys. Chem. C* **2007**, *111*, 3901−3907.
(31) Pant, D.; Levinger, N. E. *J. Phys. Chem. B* **1999**, *103*, 7846−7852.
(32) Pant, D.; Levinger, N. E. *Chem. Phys. Lett.* **1998**, *292*, 200−206.
(33) Shirota, H.; Horie, K. *J. Phys. Chem. B* **1999**, *103*, 1437−1443.
(34) Pileni, M. P.; Zemb, T.; Petit, C. *Chem. Phys. Lett.* **1985**, *118*, 414−420.
(35) Pileni, M. P.; Brochette, P.; Hickel, B.; Lerebours, B. *J. Colloid Interface Sci.* **1984**, *98*, 549−554.
(36) Pileni, M. P. *J. Phys. Chem.* **1993**, *97*, 6961−6973.
(37) Kinugasa, T.; Kondo, A.; Nishimura, S.; Miyauchi, Y.; Nishii, Y.; Watanabe, K.; Takeuchi, H. *Colloids Surf., A* **2002**, *204*, 193−199.
(38) Vasquez, V. R.; Williams, B. C.; Graeve, O. A. *J. Phys. Chem. B* **2011**, *115*, 2979−2987.
(39) Piletic, I. R.; Tan, H. S.; Fayer, M. D. *J. Phys. Chem. B* **2005**, *109*, 21273−21284.
(40) Abel, S.; Sterpone, F.; Bandyopadhyay, S.; Marchi, M. *J. Phys. Chem. B* **2004**, *108*, 19458−19466.